Organic & Biomolecular Chemistry

PAPER

View Article Online
View Journal

Substituent effects on the turn-on kinetics of rhodamine-based fluorescent pH probes†

Cite this: DOI: 10.1039/c3ob42089b

William L. Czaplyski, Grace E. Purnell, Courtney A. Roberts, Rebecca M. Allred and Elizabeth J. Harbron*

Fluorescent turn-on probes based on a rhodamine spirolactam (RSL) structure have recently become a popular means of detecting pH, metal ions, and other analytes of interest. RSLs are colorless and non-fluorescent until the target analyte induces opening of the spirocyclic ring system, revealing the fully conjugated and highly fluorescent rhodamine dye. Among RSLs opened by acid, we have observed wide variation in the kinetics of the fluorescence turn-on process such that some probes would not be usable in situations where a rapid reading is desired or the pH fluctuates temporally. Herein we present a systematic investigation of the fluorescence turn-on kinetics of RSLs to probe the hypothesis that the reaction rates are influenced by the electronic properties of the spirolactam ring system. A series of 8 aniline-derived RSLs with *para* substituents ranging from electron-donating to electron-withdrawing was prepared from rhodamine B. The fluorescence turn-on rates are observed to increase by a factor of four as the substituent is tuned from methoxy to nitro. This effect is explained in terms of the destabilization of the reaction intermediate by the substituent. As the reaction rates increase across the series, a concomitant increase in fluorescence intensity is also observed. This result is attributed to an increase in the concentration of the fluorescent form of the dye and is consistent with the expected equilibrium properties of this system. These findings are applied to the design of a faster-reacting and more intensely fluorescent RSL pH probe.

Received 20th October 2013,
Accepted 21st November 2013

DOI: 10.1039/c3ob42089b

www.rsc.org/obc

Introduction

The use of fluorescent probes to measure pH is particularly suited to samples in which the pH may be spatially or temporally heterogeneous, such as cells. Fluorescent probes for intracellular environments have been designed to respond to small differences in pH levels within two distinct regions, neutral (*ca.* pH 7) and acidic (pH 4.5–6). While a wide variety of fluorescent probes for the neutral region exist, many fewer have been developed for the acidic region.[1] Organelles including endosomes and lysosomes function within this acidic pH range, and fluorescent probes specifically designed for acidic pH levels are required to track processes within these organelles.[2]

We are interested in developing fluorescent pH probes for the acidic region based on a rhodamine spirolactam (RSL) structure. RSLs such as **1c–8c** (Scheme 1, where c denotes closed) are easily prepared from commercially available dyes such as rhodamine 6G and rhodamine B. As prepared, RSLs are colorless and non-fluorescent due to the separation of the lower xanthene core from the upper ring system by a tetrahedral spiro carbon. Acid induces a ring-opening reaction that yields a completely conjugated rhodamine dye structure. The ring-opened form is intensely colored and possesses the favorable fluorescence characteristics of a rhodamine dye[3] including high fluorescence quantum yields and good photostability. Thus, RSLs function as fluorescent turn-on probes that switch from non-fluorescent to fluorescent in response to acid stimulus.[1]

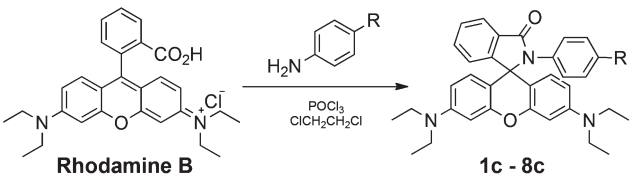

R = -OCH_3 (**1c**), -*t*-C_4H_9 (**2c**), -CH_3 (**3c**), -H (**4c**), -Cl (**5c**), -CF_3 (**6c**), -C≡N (**7c**), -NO_2 (**8c**)

Scheme 1

In recent years RSL-based pH probes have begun to appear in the literature and have thus far been applied to live cell

Department of Chemistry, The College of William and Mary, Williamsburg, Virginia 23187-8795, USA. E-mail: ejharb@wm.edu

† Electronic supplementary information (ESI) available: Derivation of eqn (2) and (4), absorption and fluorescence spectra and titration curves for probes **1–9**, ^{1}H- and ^{13}C NMR spectra of probes **1c–9c**. See DOI: 10.1039/c3ob42089b

imaging,[4–12] detection of acid vapors,[13] detection of aluminum corrosion,[14] and solution-based pH measurements.[15–19] Several studies have shown that RSLs become fluorescent in the acidic environment within lysosomes and can be used for lysosomal imaging in live cells.[4,5,8,11,12] For example, Han and coworkers demonstrated that an RSL derivative selectively stains lysosomes and has good enough photostability and retention times in cells that it can be used to monitor changes in lysosome morphology in apoptotic cells.[8] Peng and coworkers also used an RSL derivative to detect pH changes in lysosomes during apoptosis and found the performance of the RSL dye to be superior to commercially available probes.[11] These studies demonstrate the utility of RSL-based pH probes.

In our preliminary investigations of the fluorescence turn-on behavior of RSLs, we observed that some derivatives respond instantaneously to acid while others take seconds, minutes, or even longer to reach maximum fluorescence intensity at a given pH. The turn-on kinetics are critical to probe design as a slow reaction with acid renders an otherwise useful pH probe essentially unusable for many practical applications. Slow turn-on kinetics have been discussed for some RSL-based metal ion sensors,[20] but the subject has received little attention in the emerging literature of RSL pH probes. Bossi and coworkers recently explored the kinetics of ring-opening for photochromic RSLs[21] that become fluorescent in the presence of both acid and ultraviolet light.[22] They measured different thermal ring-opening rates in the presence of acid for structurally different RSLs in agreement with our own observations. We hypothesize that the rate of acid-induced ring opening of RSLs is influenced by electronic factors. To probe the role of substituent electronics in turn-on kinetics, we designed a series of aniline-derived RSLs with substituent properties ranging from electron-donating to electron-withdrawing. Herein we present the results of kinetic studies of this series as well as application of our findings to the design of a much faster-reacting probe.

Results and discussion

RSL derivatives **1c–8c** (Scheme 1) are designed to probe the influence of electronic factors on the acid-induced spirocyclic ring-opening reaction. The electronics of the spirolactam ring system are manipulated *via para* substitution of an aniline-derived phenyl ring that is attached to the spirolactam nitrogen. The selected aniline substituents span a range of electronic properties and possess Hammett σ_p constants between −0.27 (OMe) and 0.78 (NO_2).[23] Related aniline-derived rhodamine deoxy-lactams were reported by Scott and coworkers as the present manuscript was in final preparation.[24] As shown in Scheme 1, **1c–8c** were prepared from commercially available rhodamine B and the indicated anilines. The reaction proceeded *via* the rhodamine B acid chloride, which was generated *in situ* by addition of phosphorus oxychloride to a stirred solution of rhodamine B and the desired aniline. The products were obtained in 40–92% yield following purification by flash column chromatography.[25] The spiro carbon's unique resonance in the 13C NMR spectrum, observed between 67.2 and 67.6 ppm for **1c–8c**, provided verification of the spirocyclic structure.

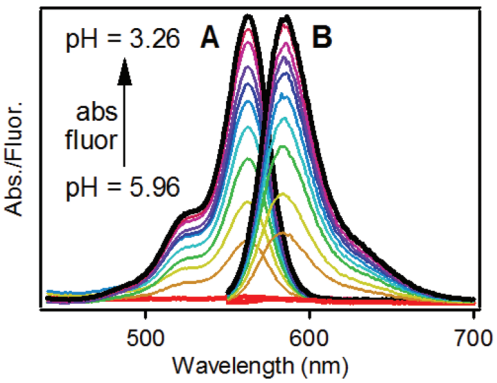

Fig. 1 Absorption (A) and fluorescence (B) of compound **8** in 1 : 1 (v/v) ethanol–water as pH is decreased from 5.96 to 3.26.

In the as-prepared spirocyclic form, **1c–8c** absorb ultraviolet light, with well-defined peaks at 315 nm and 275 nm in a 1 : 1 (v/v) solution of ethanol and water. As expected based on their non-conjugated structures, they do not absorb or fluoresce in the visible region of the spectrum. Upon introduction of HCl, a new absorbance band with a maximum around 562 nm appears, and excitation into this band yields a fluorescence spectrum with a maximum intensity around 583 nm. Fig. 1 illustrates the increase in visible absorbance and fluorescence for **8** as increasing amounts of acid are added and **8c** is converted to **8o**, where the o denotes the open form of the dye. Derivatives **1o–8o** have essentially identical absorption and fluorescence spectra, with $\lambda_{max,abs}$ and $\lambda_{max,fl}$ values each varying less than 2 nm across the series with no discernible trend with regard to substituent electronics (spectra are shown in the ESI†). The absorption and fluorescence spectra of **1o–8o** are slightly red-shifted from the parent rhodamine B dye, which has a $\lambda_{max,abs}$ of 552 nm and a $\lambda_{max,fl}$ of 580 nm in the same solvent system.

In addition to having nearly indistinguishable absorption and fluorescence spectra, **1–8** also give virtually the same fluorescence titration curves when titrated with HCl. From these titration curves, the pK_a of each derivative can be calculated by determining the pH at which probe fluorescence is half of its maximum value.[6] Fig. 2 shows the normalized titration curves for the electronic extremes of the series, **1** (OMe) and **8** (NO_2), which have pK_a values of 4.16 and 4.11, respectively. The average pK_a for the series was 4.14 ± 0.04, and the narrow distribution of values demonstrates that there are no electronic substituent effects on the pK_a. This result was somewhat surprising as we originally expected that both the pK_a and the kinetics of ring opening would be influenced by the electronic properties of the spirolactam. The uniformity in pK_a values may be a fortuitous consequence of the relationship between fluorophore concentration and rate constant, which is explored further below.

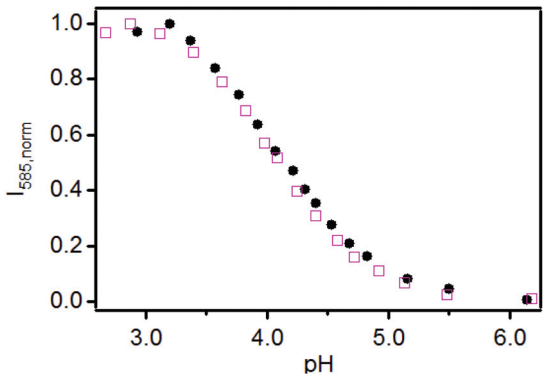

Fig. 2 Normalized fluorescence intensity at 585 nm as a function of pH for compounds **1** (circles) and **8** (squares) in 1 : 1 v/v ethanol–water.

With the similarities across the series established, we measured the kinetics of the spirocyclic ring-opening reaction by monitoring the fluorescence intensity at 585 nm as HCl was introduced to a stirring solution of each derivative. All derivatives exhibited an increase in fluorescence intensity that was consistent with first order kinetics. Fig. 3A shows kinetic traces for **1–8**, plotted in the form $\ln(I_\infty - I_t)$ *versus* time, where I_∞ and I_0 are the fluorescence intensities at times infinity and t, respectively. When plotted in this manner, first order kinetic data are linear with slope = $-k$.[26] Fig. 3A illustrates both the first order nature of the data as well as the clear variation in rate across the series. Rate constants for **1–8** are given in Table 1. The slowest kinetics are observed for **1** (OMe), and the rate of reaction increases across the series as the electron-withdrawing nature of the substituent increases. The rate constant of the fastest derivative, **8** (NO_2), is more than four times greater than that of **1**. The substituent electronics clearly impact the rate of the spirolactam ring-opening reaction.

The observed reaction kinetics can be explained by the mechanism shown in Scheme 2, which is comprised of separate protonation and ring-opening steps. Protonation of the spirolactam carbonyl yields a resonance-stabilized intermediate in which the positive charge is delocalized over oxygen, carbon, and nitrogen. Electronic rearrangement breaks down this intermediate, opening the spirolactam and producing a fully conjugated rhodamine dye. The rate constants involved in the two steps are defined in eqn (1), where CF and OF denote the closed and open forms of the dye, respectively. With 3 dye species and 4 rate constants involved, the reaction kinetics cannot be described by a simple first order expression.

$$\mathrm{CF} + \mathrm{H}^+ \underset{k_{-1}}{\overset{k_1}{\rightleftharpoons}} \mathrm{CFH}^+ \underset{k_{-2}}{\overset{k_2}{\rightleftharpoons}} \mathrm{OFH}^+ \qquad (1)$$

Rather, the rate expression for the production of the open, fluorescent form of the dye is given by eqn (2), which is derived in the ESI.†

$$[\mathrm{OFH}^+] = \frac{Q[\mathrm{D}]}{Q + k_{-2}}\left(1 - \mathrm{e}^{-(Q + k_{-2})t}\right) \qquad (2)$$

where $Q = \dfrac{k_2 k_1 [\mathrm{H}^+]}{k_{-1} + k_1 [\mathrm{H}^+]}$ and $[\mathrm{D}] = [\mathrm{CF}] + [\mathrm{CFH}^+] + [\mathrm{OFH}^+]$.

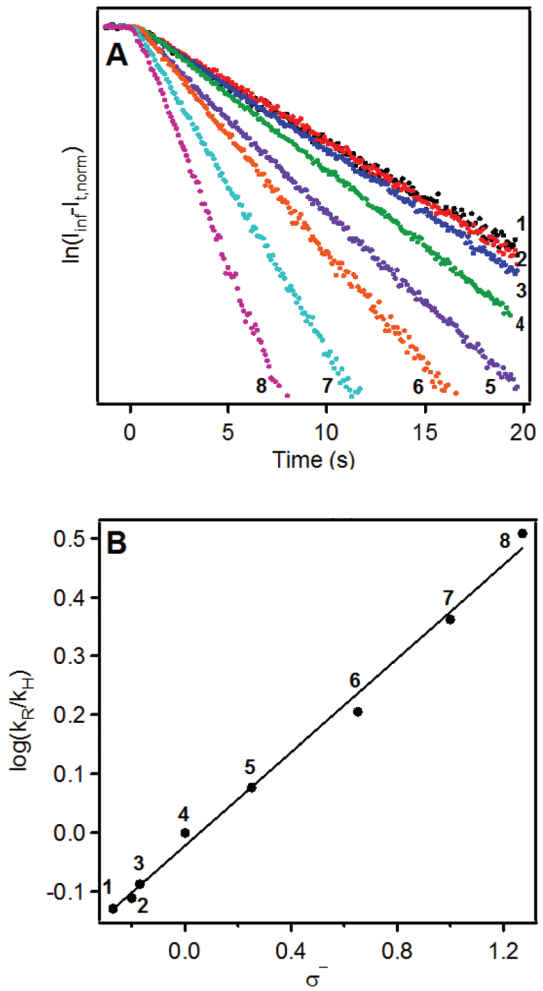

Fig. 3 (A) Kinetic data for compounds **1–8** in 1 : 1 (v/v) ethanol–water. Acid was added to the solutions at time = 0 s. (B) Hammett plot of the log of the relative rate constant *versus* σ^-.

Table 1 Rate constants and relative fluorescence intensity and absorbance

Derivative	σ^-	k_R (s^{-1})	I_R/I_H	A_R/A_H
1 $-OCH_3$	−0.27	0.0240 ± 0.0009	0.23	0.53
2 $-t\text{-}C_4H_9$	−0.20	0.0250 ± 0.0016	0.61	0.53
3 $-CH_3$	−0.17	0.0264 ± 0.0008	0.72	0.70
4 –H	0	0.0323 ± 0.0007	1.00	1.00
5 –Cl	0.25	0.0386 ± 0.0012	1.34	1.39
6 $-CF_3$	0.65	0.0518 ± 0.0017	4.96	4.84
7 –CN	1	0.0745 ± 0.0017	5.27	5.06
8 $-NO_2$	1.27	0.1041 ± 0.0021	3.89	5.60

Eqn (2) demonstrates that the observed first order rate constant, k, incorporates all 4 rate constants from eqn (1) as well as the concentration of acid (*i.e.*, $k = Q + k_{-2}$). Given that k_1 and k_{-1} are expected to be rapid[22] and essentially the same for all derivatives and $[H^+]$ is identical in all kinetic experiments, the observed differences in k arise from structure-dependent differences in k_2 and k_{-2}. Bossi and coworkers previously estimated k_{-2} for a different series of RSLs and found it to be

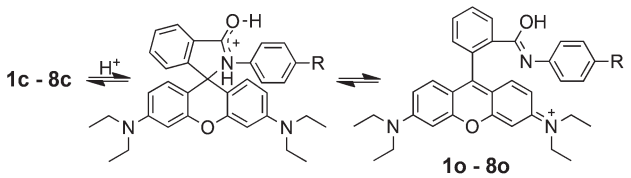

R = -OCH_3 (**1**), -*t*-C_4H_9 (**2**), -CH_3 (**3**), -H (**4**), -Cl (**5**), -CF_3 (**6**), -C≡N (**7**), -NO_2 (**8**)

Scheme 2

approximately equal for their compounds.[22] If the same is true here, then differences in the observed k would be dominated by k_2.

A Hammett analysis further demonstrates the relationship between substituent electronics and ring-opening reaction kinetics in this system. We initially plotted the log of the relative rate constant *versus* σ_p and observed a linear correlation of rate constants with electron-donating and weakly electron-withdrawing substituents (not shown). Deviations from linearity were observed for the strongly electron-withdrawing substituents, which exhibited rate constants that were larger than predicted. Fig. 3B shows the revised Hammett plot with the log of the relative rate constant *versus* σ^-, the Hammett substituent constant used when resonance between the reaction site and electron-withdrawing substituents is important.[23,27] This plot is linear across all substituents (r = 0.997) and gives reaction constant ρ = 0.40 ± 0.01. A positive reaction constant for this system indicates that positive charge is diminished during the course of the reaction. This information is consistent with Scheme 2, where the positively-charged intermediate is transformed to the rhodamine form of the dye during the rate-determining reaction step. Electron-withdrawing substituents destabilize the positively-charged intermediate both inductively and *via* resonance, where possible, while electron-donating substituents have the opposite effect. Electronic destabilization of the intermediate is expected to accelerate k_2.

The Hammett analysis implies that the RSL substituents affect the rate of ring-opening by altering the electronics of the spirolactam ring. Additional support for this idea comes from NMR evidence that the electronic environment of the spirolactam ring does indeed change as a function of the substituent. Fig. 4 shows the ^{13}C NMR chemical shifts of the carbonyl carbon for each derivative in its closed form (**1c–8c**) *versus* σ^-. The chemical shift values are clearly correlated with the substituent constants: the carbonyl carbon becomes deshielded as the electron-withdrawing power of the substituent increases. The trend is not as linear as in Fig. 3B, and substituents *tert*-butyl (**2**) and methyl (**3**) were included in the series so that the potential role of steric interactions in the scatter could be explored. In terms of the ring-opening reaction, steric effects derived from the *para* substituents do not appear to play a role as **2** and **3** both yielded nearly identical rate constants consistent with their extremely similar σ^- values (Fig. 3B, Table 1). In contrast, the carbonyl chemical shift of **2c** deviates noticeably from **3c**, which is more in line with the other substituents with

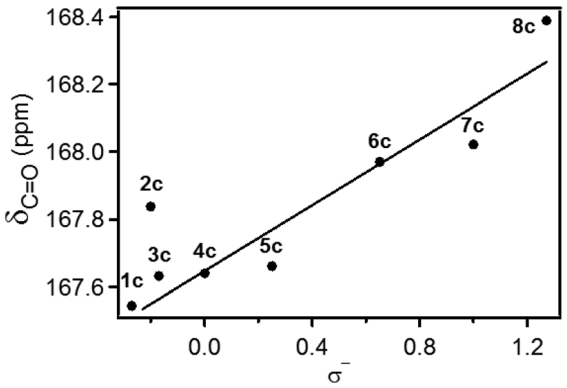

Fig. 4 Chemical shift of the carbonyl carbons of **1c–8c** in $CDCl_3$ *versus* σ^-.

σ^- < 0.4. The chemical environment thus appears to be affected by steric interactions in addition to the expected influence of substituent electronics; these complex influences on the chemical environment may explain the scatter observed in Fig. 4. When **2c** is excluded from the analysis, a linear fit of chemical shift *versus* σ^- gives r = 0.959. Overall, the general correlation of carbonyl chemical shift with σ^- demonstrates that spirolactam electronics can be manipulated by the substituents in a predictable way.

The consequences of the tunable ring-opening kinetics observed here extend beyond just reaction rates. The ideal fluorescent pH probe would not only have a fast response to pH change but also be bright and, therefore, easy to detect. Table 1 presents the peak fluorescence intensities at pH 3 of **1o–8o** relative to unsubstituted **4o**, and the data demonstrate surprising variation across the series. The most intense derivative, **7o** (CN), is nearly 23 times more intense than the dimmest, **1o** (OMe). With the exception of **8o** (NO_2), the fluorescence intensities increase as the electron-withdrawing nature of the substituent increases. Thus, the fastest-reacting probes are also the brightest. The reason for this dramatic variation in fluorescence intensity becomes apparent upon examination of the relative peak absorbance values for **1o–8o**, also measured at pH 3 and shown in Table 1. The fluorescence intensities of derivatives **2o–7o** are highly correlated with their absorbances. Derivatives **1o** (OMe) and **8o** (NO_2) both have lower fluorescence intensities than predicted by their absorbances, an effect that may be due to substituent-specific effects on the fluorescence quantum yield. Absorbance varies by a factor of 10 across the series, and, according to Beer's Law, this trend can only be due to a substituent-dependent variation in extinction coefficient or concentration. Given the improbability that substitution of the same chromophore could cause such a large difference in extinction coefficients, concentration differences emerge as the most likely explanation for this trend.

The apparent increase in probe concentration with increasing electron-withdrawing nature of the substituent is unexpected as **1–8** all have essentially the same pK_a. According to the standard Henderson-Hasselbalch equation (eqn (3)),

concentrations of the two forms of an acid-base indicator, In and HIn^+, are equal when pH = pK_a. Our observed results clearly fail to match this expectation as the variation in absorbance is the same whether measured at pH = pK_a or other pH values.

$$\mathrm{pH} = \mathrm{p}K_a + \log\left(\frac{[\mathrm{In}]}{[\mathrm{HIn}^+]}\right) \quad (3)$$

Eqn (3) applies to a typical pH indicator that has only 2 forms, one colorless and one colored. As shown in Scheme 2 and eqn (1), RSL-based indicators are more complex, with two colorless species (CF and CFH^+) and one colored species (OFH^+). Given the Scheme 2 mechanism and standard equilibrium assumptions, a new expression relating pH, pK_a, and probe concentrations can be derived for this 3-species scenario (derivation shown in ESI†). The result is given as eqn (4), where the terms were defined in eqn (1).

$$\mathrm{pH} = \mathrm{p}K_a + \log\left(\frac{k_2[\mathrm{CF}]}{k_{-2}[\mathrm{OFH}^+]}\right) \quad (4)$$

Not only species concentrations but also rate constants appear in this expression. As discussed previously, our measured rate constants represent the sum of k_{-2} and an expression involving k_2, which complicates comparison of experimental data to eqn (4), in which k_2 and k_{-2} appear as a simple ratio. The observed rate constant increases by a factor of 4 as the concentration of OFH^+, represented by absorbance, increases by a factor of 10 across the series **1–8**. This result is in agreement with the correlated increase of k_2 and concentration of open form predicted by eqn (4). The variation in magnitude of increase between rate constant and absorbance is most likely due to the complexity of what the measured k represents and/or small variations in extinction coefficients among the derivatives. Eqn (4) supports our conclusion that the fastest-reacting derivatives are also the brightest. Correlation of rate constant with equilibrium constant for another series of RSL derivatives has also been observed by Bossi.[22]

Having established that the fastest-reacting and brightest probes are those with electron-withdrawing substituents on the spirolactam ring, we next applied this finding to the design of an RSL pH probe with superior properties. Probe **9**, shown in its open form below, is derived from 2,6-dichloro-4-nitroaniline, which is expected to exert a much stronger electron-withdrawing substituent effect on the spirolactam moiety than **8**, which bears only the nitro substituent.

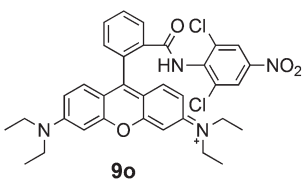

9o

Fig. 5 shows the kinetic trace for **9** along with **8**, the fastest-reacting of the original series, for reference. The kinetics of **9** are significantly faster than those observed for the original

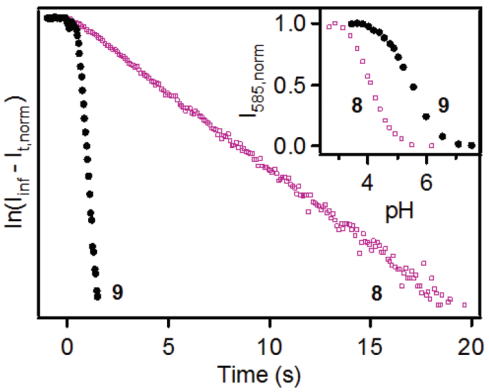

Fig. 5 Kinetic data for compounds **8** (squares) and **9** (circles) in 1 : 1 (v/v) ethanol–water. Acid was added to the solutions at time = 0 s. Inset: normalized peak fluorescence intensity at 585 nm as a function of pH for compounds **8** (squares) and **9** (circles).

series. At early times following the addition of acid, the kinetics of **9** are well-described by first order kinetics, as can be seen by the linear nature of the trace in Fig. 5. The kinetics at later times deviate from first order, an effect that could be due to the additional steric constraints of **9** as compared to **1–8**. A first order fit of the early-time data for **9** yields a rate constant that is more than 16 times faster than **8**. In practical terms, the observed kinetics represent the difference between an acceptably fast ring-opening for **8** with half of the fluorescence appearing in just over 6 s and an almost instantaneous reaction for **9** with half of the fluorescence appearing in under 1 s. In addition to rapid ring-opening kinetics, **9o** also possesses a fluorescence intensity exceeding that of **1o–8o**. Relative to **4o**, its fluorescence intensity is 6.67, which makes it the brightest of the RSLs studied here. The concentration of **9o** as expressed by its absorbance is even higher at 10.43 relative to **4o**. It appears at the highest concentration and greatest fluorescence intensity of all of the derivatives though, like **8o** (NO_2), its fluorescence is less intense than predicted by absorbance.

Our finding that electron withdrawing substituents accelerate the ring-opening kinetics of **9** indicates that the powerful electron-withdrawing effect of the one nitro and two chloro substituents is at least partially responsible for its fast reaction. However, unfavorable steric interactions due to the *ortho* substituents in **9** most likely also play a role in the rapid kinetics. Titration of **9** reveals that it has a pK_a of 5.43, which is distinctly higher than the average pK_a of 4.14 observed for **1–8**. The Fig. 5 inset demonstrates the significant difference in titration response between **9** and **8**, again selected as a reference. Lin and coworkers previously demonstrated that RSL pK_a values can be increased by functionalizing the spirolactam nitrogen with substituents that are extremely sterically demanding, such as adamantyl.[7] Although pK_a and kinetics are separate issues, it seems likely that unfavorable steric interactions that are significant enough to shift the pK_a of **9** also play a role in its rapid ring-opening kinetics. We can estimate the extent to which **9**'s fast response is due to electronic *versus* steric factors by evaluating **9** in terms of the Hammett plot for

1–8. An estimated Hammett constant for the 2,4-dichloro-6-nitro moiety was calculated by adding together Traynham's σ_o value of 0.50 for each of the *o*-chloro substituents and the σ^- value for the *p*-nitro substituent to yield 2.27.[28] We used this Hammett constant value and the ρ calculated for Fig. 3B to determine an expected rate constant for **9** based solely upon the electronics of its substituents. This analysis yielded a value of 0.25 s^{-1} for the rate constant, while the actual value of 1.74 s^{-1} is nearly 7 times greater in magnitude. Thus, the majority of **9**'s fast response is likely due to unfavorable steric factors while a smaller proportion is attributable to the strong electron-withdrawing effect of the substituents. Nevertheless, our findings regarding the kinetics of spirolactam ring opening enabled us to design the fastest-reacting and most intensely fluorescent probe of this series.

Conclusions

Rate of response to the desired analyte is a key figure of merit for any fluorescent turn-on probe. We have demonstrated that pH probes based on a rhodamine spirolactam structure convert from non-fluorescent to fluorescent at a rate that depends on the electronics of the spirolactam ring, with the fastest fluorescence turn-on behavior observed for dyes with electron-withdrawing substituents. In addition to reaction rate, fluorescence intensity was also observed to be correlated with substituent electronics. The fastest-reacting derivatives were also the most intensely fluorescent, and this effect was due to an increase in fluorescent dye concentration. This variation in concentration was shown to originate in the 3-species equilibrium for the RSL pH probes, which creates a scenario in which larger rate constants yield larger concentrations of the fluorescent form of the dye. These findings were used to design a faster-reacting, more intensely fluorescent pH probe derived from 2,4-dichloro-6-nitroaniline. This probe also had a much higher pK_a than those with only *para* substituents on the aniline (5.43 *vs.* 4.14) in agreement with the findings of Lin that sterically demanding substituents raise the pK_a of RSL-based pH probes.[7] Collectively, these results demonstrate that RSLs can be easily functionalized to furnish rapid-reacting pH probes that are responsive within the so-called acidic window.

Experimental section

Absorbance and fluorescence studies

Absorbance and fluorescence measurements were made on a Varian Cary50 and Varian Eclipse, respectively. Stock solutions of **1c–9c** were prepared in 1 : 1 (v/v) ethanol–water at a concentration of 7.7 μM (**1–5**) or 0.077 μM (**6–9**) and were stirred at room temperature for 1 h prior to absorbance and fluorescence studies.[16] Data for compounds **6–9** were corrected for the additional dilution to facilitate comparison with **1–5**. For kinetic measurements, 2 M HCl was added to a cuvette containing a stirring solution of **1c–9c** while the fluorescence intensity at 585 nm was monitored upon 535 nm excitation. The acid concentration in the cuvette was 6.6 mM, and the pH was 2.7. Reported rate constants are the average of a minimum of 9 total kinetic runs from at least 3 different samples. Absorption and fluorescence titrations were conducted by adding small aliquots of 2 M HCl to a stirring stock solution (100 mL) of **1c–9c**. Aliquots were removed for spectroscopic measurement (fluorescence λ_{exc} = 535 nm) after the pH stabilized and were then returned to the stock solution.

Materials and methods

All reactions were carried out with flame-dried glassware under an argon atmosphere. Reagents were purchased from Acros or Sigma-Aldrich and used as received. ^{1}H and proton-decoupled ^{13}C NMR spectra were recorded on a Varian Mercury 400 (^{1}H 400 MHz, ^{13}C 100 MHz) and referenced to TMS (^{1}H) or $CDCl_3$ at 77.0 ppm (^{13}C). Chemical shifts are reported in ppm and coupling constants in Hz. Mass spectra were measured through positive electrospray ionization (w/NaCl) on a Bruker 12 Tesla APEX-Qe FTICR-MS with and Apollo II ion source.

General procedure for the synthesis of compounds 1c–9c

To a stirred solution of rhodamine B (0.21 mmol) and the desired aniline (0.63 mmol) in 1,2-dichloroethane (5 mL) at 0 °C, phosphorus oxychloride (0.25 mmol) was added dropwise under argon atmosphere. The mixture was stirred at 0 °C for 15 min, heated to 85 °C for 5 h, and then cooled to room temperature. The solution was diluted with chloroform (20 mL) and acidified with 2 M HCl (30 mL). The organic layer was washed with additional 2 M HCl (2 × 30 mL), 2 M NaOH (3 × 30 mL), and brine (30 mL). The organic layer was dried with Na_2SO_4 and concentrated *in vacuo*.

1c: Compound **1c** was reported previously.[24] The brown oil was purified by flash column chromatography on silica gel (elution: 40% to 60% EtOAc in hexanes) to afford **1** (72.8 mg, 64% yield) as a pale tan solid: TLC (40% EtOAc in hexanes) R_f: 0.45 (UV); ^{1}H NMR (400 MHz, $CDCl_3$) 8.01 (m, 1H), 7.50–7.48 (t, *J* = 3.5 Hz, 2H), 7.18–7.16 (m, 1H), 6.64–6.60 (m, 6H), 6.33–6.30 (dd, *J* = 8.8, 2.5 Hz, 2H), 6.25–6.24 (d, *J* = 2.3 Hz, 2H), 3.67 (s, 3H), 3.35–3.29 (qd, *J* = 7.0, 2.7 Hz, 8H), 1.16–1.13 (t, *J* = 7.0 Hz, 12H); ^{13}C NMR (100 MHz, $CDCl_3$) 167.5, 158.1, 153.1, 152.9, 148.6, 132.6, 131.3, 128.95, 128.85, 128.0, 124.0, 123.2, 113.8, 107.9, 106.2, 97.6, 67.3, 55.1, 44.2, 12.5; HRMS (ES+): Exact mass calcd for $C_{35}H_{37}N_3O_3$ $[M + Na]^+$, 570.2727. Found 570.2729.

2c: The brown solid was purified by flash column chromatography on silica gel (elution: 5% to 40% EtOAc in hexanes) and trituration from hexanes to afford **2** (111.4 mg, 94% yield) as a white powder: TLC (20% EtOAc in hexanes) R_f: 0.35 (UV); ^{1}H NMR (400 MHz, $CDCl_3$) 7.99 (m, 1H), 7.47–7.45 (t, *J* = 3.5 Hz, 2H), 7.13–7.11 (m, 3H), 6.78–6.76 (d, *J* = 8.2 Hz, 2H), 6.66–6.64 (d, *J* = 8.6 Hz, 2H), 6.32–6.29 (d, *J* = 9.0 Hz, 2H), 6.28 (s, 2H), 3.32–3.31 (m, 8H), 1.20 (s, 9H), 1.16–1.13 (t, *J* = 7.0 Hz, 12H); ^{13}C NMR (100 MHz, $CDCl_3$) 167.8, 153.5, 152.9, 148.9,

148.6, 133.8, 132.7, 130.7, 128.8, 127.9, 126.3, 125.4, 123.8, 123.2, 108.0, 105.5, 97.7, 67.2, 44.2, 34.3, 31.2, 12.5, 1.0; HRMS (ES+): Exact mass calcd for $C_{38}H_{43}N_3O_2$ $[M + Na]^+$, 596.3247. Found 596.3250.

3c: Compound **3c** was reported previously.[24] The red oil was purified by flash column chromatography on silica gel (elution: 0% to 2% MeOH in $CHCl_3$) to afford a brown solid residue. Trituration with Et_2O yielded **3** (89.1 mg, 40% yield) as a pale tan powder: TLC (2% MeOH in $CHCl_3$) R_f: 0.25 (UV); ^{1}H NMR (400 MHz, $CDCl_3$) 8.02–7.99 (m, 1H), 7.50–7.46 (m, 2H), 7.16–7.15 (m, 1H), 6.93–6.91 (d, J = 7.0 Hz, 2H), 6.66–6.64 (d, J = 8.2 Hz, 4H), 6.33–6.30 (d, J = 8.6 Hz, 2H), 6.26 (s, 2H), 3.34–3.29 (q, J = 7.0 Hz, 8H), 2.21 (d, J = 1.2 Hz, 3H), 1.17–1.13 (t, J = 7.0 Hz, 12H); ^{13}C NMR (100 MHz, $CDCl_3$) 167.6, 153.2, 153.1, 148.6, 136.3, 133.7, 132.6, 131.1, 129.2, 128.9, 128.0, 127.3, 123.9, 123.3, 108.0, 106.4, 97.7, 67.2, 44.3, 21.1, 12.5; HRMS (ES+): Exact mass calcd for $C_{35}H_{37}N_3O_2$ $[M + Na]^+$, 554.2778. Found 554.2779.

4c: Compound **4c** was reported previously.[22,24] The brown solid was purified by flash column chromatography on silica gel (elution: 40% to 50% EtOAc in hexanes) to afford **4** (58.4 mg, 54% yield) as a white powder: TLC (40% EtOAc in hexanes) R_f: 0.60 (UV); ^{1}H NMR (400 MHz, $CDCl_3$) 8.00 (m, 1H), 7.50 (m, 2H), 7.17–7.16 (m, 2H), 7.12 (m, 3H), 6.81–6.78 (d, J = 6.6 Hz, 2H), 6.65–6.63 (dd, J = 8.6/1.6 Hz, 2H), 6.31–6.29 (d, J = 9.0 Hz, 2H), 6.25 (s, 2H), 3.34–3.29 (q, J = 7.2 Hz, 8H), 1.16–1.3 (t, J = 7.0 Hz, 12H); ^{13}C NMR (100 MHz, $CDCl_3$) 167.6, 153.2, 153.1, 148.7, 136.6, 132.8, 131.0, 128.8, 128.5, 128.1, 127.3, 126.6, 124.0, 123.3, 108.0, 106.4, 97.7, 67.4, 44.3, 12.5; HRMS (ES+): Exact mass calcd for $C_{34}H_{35}N_3O_2$ $[M + Na]^+$, 540.2621. Found 540.2623.

5c: Compound **5c** was reported previously.[24] The brown oil was purified by flash column chromatography on silica gel (elution: 0% to 4% MeOH in $CHCl_3$) to afford **5** (114.6 mg, 50% yield) as a tan solid: TLC (2% MeOH in $CHCl_3$) R_f: 0.25 (UV); ^{1}H NMR (400 MHz, $CDCl_3$) 8.00 (m, 1H), 7.50–7.48 (m, 2H), 7.15 (m, 1H), 7.11–7.08 (dd, J = 8.8, 2.5 Hz, 2H), 6.80–6.77 (dd, J = 8.8, 2.1 Hz, 2H), 6.63–6.60 (dd, J = 8.8, 2.1 Hz, 2H), 6.32–6.28 (m, 4H), 3.35–3.30 (q, J = 6.9 Hz, 8H), 1.17–1.13 (t, J = 7.0 Hz, 12H); ^{13}C NMR (100 MHz, $CDCl_3$) 167.7, 153.2, 153.0, 148.7, 135.3, 133.0, 132.1, 130.6, 128.73, 128.67, 128.3, 128.2, 124.0, 123.3, 108.1, 106.0, 97.7, 67.4, 44.3, 12.5; HRMS (ES+): Exact mass calcd for $C_{34}H_{34}ClN_3O_2$ $[M + Na]^+$, 574.2232. Found 574.2234.

6c: Compound **6c** was reported previously.[24] The red oil was purified by flash column chromatography on silica gel (elution: 0% to 2% MeOH in $CHCl_3$) to afford **6** (209 mg, 85% yield) as a pale tan solid: TLC (2% MeOH in $CHCl_3$) R_f: 0.35 (UV); ^{1}H NMR (400 MHz, $CDCl_3$) 8.01 (m, 1H), 7.47 (t, J = 3.3 Hz, 2H), 7.39–7.37 (d, J = 8.6 Hz, 2H), 7.18–7.16 (d, J = 8.2 Hz, 2H), 7.12 (m, 1H), 6.64–6.62 (d, J = 9.0 Hz, 2H), 6.33–6.32 (d, J = 2.3 Hz 2H), 6.31–6.28 (dd, J = 9.0/2.3 Hz, 2H), 3.32–3.29 (q, J = 6.8 Hz, 8H), 1.16–1.13 (t, J = 7.0 Hz, 12H); ^{13}C NMR (100 MHz, $CDCl_3$) 168.0, 153.5, 152.7, 148.7, 140.3, 133.2, 129.7, 128.4, 128.2, 127.5 (^2J = 32.4 Hz), 125.7, 125.6 (^3J = 3.7 Hz), 124.0 (^1J = 272 Hz), 123.8, 123.3, 108.1, 105.8, 97.7, 67.3, 44.2, 12.4; HRMS (ES+): Exact mass calcd for $C_{35}H_{34}F_3N_3O_2$ $[M + Na]^+$, 608.2495. Found 608.2497.

7c: The magenta oil was purified by flash column chromatography on silica gel (elution: 0% to 5% MeOH in $CHCl_3$) to afford **7** (208.3 mg, 92% yield) as a tan solid: TLC (2% MeOH in $CHCl_3$) R_f: 0.30 (UV); ^{1}H NMR (400 MHz, $CDCl_3$) 7.98 (d, J = 6.3 Hz, 1H), 7.45–7.43 (m, 2H), 7.37–7.36 (d, J = 7.0 Hz, 2H), 7.28–7.26 (d, J = 8.6 Hz, 2H), 7.08 (d, J = 6.3 Hz, 1H), 6.58–6.56 (d, J = 9.0 Hz, 2H), 6.34–6.33 (d, J = 2.0 Hz, 2H), 6.27–6.24 (d, J = 9.0 Hz, 2H), 3.32–3.27 (q, J = 6.6 Hz, 8H), 1.15–1.11 (t, J = 6.6 Hz, 12H); ^{13}C NMR (100 MHz, $CDCl_3$) 168.0, 153.5, 152.5, 148.7, 141.5, 133.4, 132.3, 129.1, 128.1, 128.0, 124.9, 123.7, 123.3, 118.7, 108.4, 108.1, 105.6, 97.6, 67.3, 44.1, 12.4; HRMS (ES+): Exact mass calcd for $C_{35}H_{34}N_4O_2$ $[M + Na]^+$, 565.2574. Found 565.2576.

8c: The red oil was purified by flash column chromatography on silica gel (elution: 40% to 50% EtOAc in hexanes) to afford **8** (97.2 mg, 83% yield) as a yellow solid: TLC (40% EtOAc in hexanes) R_f: 0.70 (UV); ^{1}H NMR (400 MHz, $CDCl_3$) 8.01–7.99 (m, 3H), 7.53–7.46 (m, 2H), 7.40–7.37 (dd, J = 7.0, 2.0 Hz, 2H), 7.11 (d, J = 6.6 Hz, 1H), 6.58–6.56 (d, J = 8.6 Hz, 2H), 6.34–6.33 (d, J = 2.7 Hz, 2H), 6.27–6.24 (dd, J = 8.8, 2.5 Hz, 2H), 3.34–3.29 (q, J = 7.0 Hz, 8H), 1.17–1.13 (t, J = 7.0 Hz, 12H); ^{13}C NMR (100 MHz, $CDCl_3$) 168.4, 153.8, 152.6, 148.9, 144.4, 143.6, 133.7, 129.0, 128.3, 128.1, 124.4, 124.0, 123.8, 123.5, 108.2, 105.7, 97.7, 67.6, 44.3, 12.5; HRMS (ES+): Exact mass calcd for $C_{34}H_{34}N_4O_4Na$ $[M + Na]^+$, 585.2472. Found 585.2474.

9c: The purple solid was purified by flash column chromatography on silica gel (elution: 0% to 3% MeOH in $CHCl_3$) to afford **9** (161.3 mg, 61% yield) as an orange solid: TLC (2% MeOH in $CHCl_3$) R_f: 0.30 (UV); ^{1}H NMR (400 MHz, $CDCl_3$) 8.07 (d, J = 7.8 Hz, 1H), 8.0 (d, J = 1.2 Hz, 1H), 7.71 (t, J = 7.4 Hz, 1H), 7.65 (t, J = 7.4 Hz, 1H), 7.41 (d, J = 7.4 Hz, 1H), 7.26 (d, J = 6.6 Hz, 1H), 6.61–6.58 (d, J = 9.0 Hz, 2H), 6.31–6.28 (dd, J = 9.0, 2.3 Hz), 6.23 (d, J = 2.0 Hz, 2H), 3.36–3.30 (q, J = 7.0 Hz, 8H), 1.16–1.12 (t, J = 6.8 Hz, 12H); ^{13}C NMR (100 MHz, $CDCl_3$) 196.0, 155.4, 149.5, 149.3, 146.9, 138.7, 138.4, 133.0, 132.0, 130.3, 128.9, 124.9, 124.0, 123.1, 107.6, 107.4, 97.9, 71.2, 44.4, 12.4; HRMS (ES+): Exact mass calcd for $C_{34}H_{32}Cl_2N_4O_4$ $[M + Na]^+$, 653.1693. Found 653.1698.

Acknowledgements

We gratefully acknowledge support of this work by the Camille and Henry Dreyfus Foundation through a Henry Dreyfus Teacher-Scholar Award and by the William and Mary Women in Scientific Education (WISE) Initiative supported by the National Science Foundation. R.M.A. thanks the Charles Center of the College of William and Mary for support *via* an Honors Fellowship. Partial support for this work was provided by student research fellowships to W.L.C. and C.A.R. from the Howard Hughes Medical Institute Undergraduate Science Education grant to the College of William and Mary.

References

1 X. Chen, T. Pradhan, F. Wang, J. S. Kim and J. Yoon, *Chem. Rev.*, 2012, **112**, 1910.
2 J. Han and K. Burgess, *Chem. Rev.*, 2009, **110**, 2709.
3 M. Beija, C. A. M. Afonso and J. M. G. Martinho, *Chem. Soc. Rev.*, 2009, **38**, 2410.
4 H. Li, H. Guan, X. Duan, J. Hu, G. Wang and Q. Wang, *Org. Biomol. Chem.*, 2013, **11**, 1805.
5 T. Hasegawa, Y. Kondo, Y. Koizumi, T. Sugiyama, A. Takeda, S. Ito and F. Hamada, *Biorg. Med. Chem.*, 2009, **17**, 6015.
6 W. Zhang, B. Tang, X. Liu, Y. Liu, K. Xu, J. Ma, L. Tong and G. Yang, *Analyst*, 2009, **134**, 367.
7 L. Yuan, W. Lin and Y. Feng, *Org. Biomol. Chem.*, 2011, **9**, 1723.
8 Z. Li, S. Wu, J. Han and S. Han, *Analyst*, 2011, **136**, 3698.
9 Z.-Q. Hu, M. Li, M.-D. Liu, W.-M. Zhuang and G.-K. Li, *Dyes Pigm.*, 2013, **96**, 71.
10 N. B. Yapici, S. R. Mandalapu, T.-L. Chew, S. Khuon and L. Bi, *Bioorg. Med. Chem. Lett.*, 2012, **22**, 2440.
11 H. Zhu, J. Fan, Q. Xu, H. Li, J. Wang, P. Gao and X. Peng, *Chem. Commun.*, 2012, **48**, 11766.
12 S. Wu, Z. Li, J. Han and S. Han, *Chem. Commun.*, 2011, **47**, 11276.
13 S. Kang, S. Kim, Y.-K. Yang, S. Bae and J. Tae, *Tetrahedron Lett.*, 2009, **50**, 2010.
14 A. Augustyniak and W. Ming, *Prog. Org. Coat.*, 2011, **71**, 406.
15 M. Tian, X. Peng, J. Fan, J. Wang and S. Sun, *Dyes Pigm.*, 2012, **95**, 112.
16 Q. A. Best, R. Xu, M. E. McCarroll, L. Wang and D. J. Dyer, *Org. Lett.*, 2010, **12**, 3219.
17 V. B. Bojinov, A. I. Venkova and N. I. Georgiev, *Sens. Actuators, B*, 2009, **143**, 42.
18 J. Hu, L. Dai and S. Liu, *Macromolecules*, 2011, **44**, 4699.
19 M. Adamczyk and J. Grote, *Bioorg. Med. Chem. Lett.*, 2003, **13**, 2327.
20 K. Sreenath, R. J. Clark and L. Zhu, *J. Org. Chem.*, 2012, **77**, 8268.
21 V. N. Belov and M. L. Bossi, *Isr. J. Chem.*, 2013, **53**, 267.
22 H. Montenegro, M. Di Paolo, D. Capdevila, P. F. Aramendia and M. L. Bossi, *Photochem. Photobiol. Sci.*, 2012, **11**, 1081.
23 C. Hansch, A. Leo and R. W. Taft, *Chem. Rev.*, 1991, **91**, 165.
24 Q. A. Best, C. Liu, P. D. van Hoveln, M. E. McCarroll and C. N. Scott, *J. Org. Chem.*, 2013, **78**, 10134.
25 W. C. Still, M. Kahn and A. Mitra, *J. Org. Chem.*, 1978, **43**, 2923.
26 K. A. Connors, *Chemical Kinetics: The Study of Reaction Rates in Solution*, VCH, New York, 1990.
27 H. H. Jaffé, *Chem. Rev.*, 1953, **53**, 191.
28 M. T. Tribble and J. G. Traynham, *J. Am. Chem. Soc.*, 1969, **91**, 379.

